ГОДИШНИК НА УНИВЕРСИТЕТА ПО АРХИТЕКТУРА, СТРОИТЕЛСТВО И ГЕОДЕЗИЯ – СОФИЯ

ANNUAL OF THE UNIVERSITY OF ARCHITECTURE, CIVIL ENGINEERING AND GEODESY – SOFIA

XLIII и XLIV том vol. 2004–2009 св. fasc. II

MODELLING INTERGRANULAR CRACK PROPAGATION TO AID MICROSTRUCTURE ENGINEERING. PART II: RESULTS

A. Jivkov[1]

Keywords: *intergranular cracking, stainless steels, microstructure, grain boundaries, crack bridging, finite element analysis*

MSC 2000: *74R10*

ABSTRACT

The presents paper the results for crack propagation in the 3D microstructure model for a series of experimentally observed fractions of resistant boundaries. Results demonstrate the formation of bridging ligaments by the resistant boundaries and their influence on the crack driving force. It is shown that increasing the fraction of resistant grain boundaries increased the degree of crack tip shielding developed. The crack tip shielding is expected to reduce the crack propagation rate, hence to increase the material resistance to intergranular cracking. The 2D microstructure model is used for simulations with random distribution of boundaries and a series of susceptible and resistant boundaries failure strengths. The influence of stress on crack path and the influence of the susceptible and resistant boundaries failure strengths on crack behaviour are demonstrated. The effects of crack bridging and crack branching are quantified. It is concluded that the fraction and the failure characteristics of the resistant boundaries are the parameters controlling the shielding effect of bridges.

[1] Andrey Jivkov, The University of Manchester, School of Materials, Grosvenor Street, Manchester M1 7HS, UK; Tel: +44 (0)161 3063556; Fax: +44 (0)161 3063586; E-mail: andrey.jivkov@manchester.ac.uk

1. Introduction

In the framework of the proposed model, the microstructure effects on IGEAC could be studied by a series of simulations with variable strengths of the susceptible and the resistant boundaries, and a variable fraction of the random distribution of resistant and susceptible boundaries. The aim with such a series would be to answer the following questions:

- Do the observed resistant boundaries control crack growth by dissipating energy in plastic deformation, or are they just energetically unimportant remnants left by crack propagation?

- How does this answer change with the strength and fraction of susceptible and resistant boundaries?

In the 3D cases studied here one crack propagation simulation for given fraction, distribution and properties of the grain boundaries required typically seven to ten days of computation time on a personal computer. Therefore, the results presented in this work do not cover the influences of all model parameters. The aim of the 3D solutions conducted so far has been to demonstrate that the assumptions necessary for crack bridging in the 2D model are supported by the more realistic 3D implementation of the same mechanism. With the proposed 2D model, however, it was possible to accomplish a relatively large series of simulations that provide qualitative answers to the above questions.

2. Results and discussion

2.1. 3D Simulations

The 3D simulations use failure strains of the susceptible and the resistant boundaries, fixed to the values $\varepsilon_{sf} = 0.1\varepsilon_0$ and $\varepsilon_{rf} = 10\varepsilon_0$, respectively. Seven different fractions of resistant boundaries, $f = 0.20, 0.25, 0.30, 0.35, 0.40, 0.45, 0.50$, have been considered. These enclose the experimentally determined fractions, $0.25 < f < 0.40$, in microstructures of Grade 304 austenitic stainless steels, for “as received” materials and “grain boundary engineered” materials [1]. For each fraction, five random distributions of the boundaries in the assembly have been simulated. Initial simulations showed that crack arrest was not achievable for the considered microstructures at the initial applied load. Therefore, artificial termination of the computations after 200 steps was adopted in the results presented.

The images (a), (b), and (c) in Fig. 1 illustrate three stages of crack development in a microstructure with $f = 0.35$, after 50, 100 and 200 steps, respectively. Ruptured grain boundaries with different orientation are shown in different colours. Holes in the crack surface designate bridges formed during evolution. To demonstrate the crack deviation form the original crack plane, a top-down view of the crack after 200 steps is shown in Fig. 1(d).

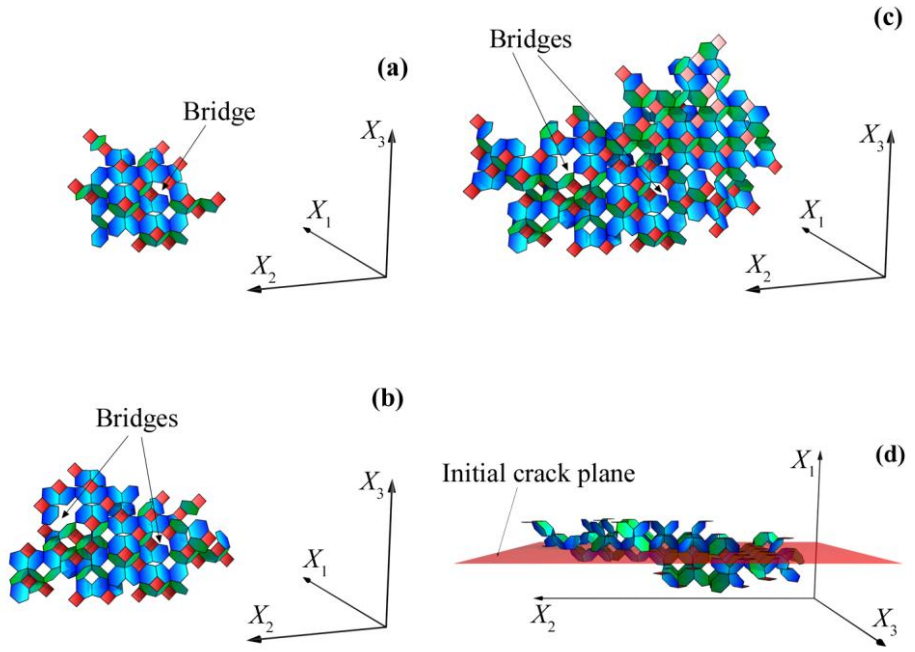

Figure 1. Growth of a single crack with bridges formation in a microstructure with f = 0.35

The total crack area, including ruptured boundaries and bridges, projected on the initial plane is denoted by A_{crack} and is taken as the independent parameter in the following figures. This crack area is measured in units D^2, noting that D is the grain size. In general, the crack's geometry in the X_2-X_3 plane was observed to be maintained very close to a semi-circular shape during evolution. An amount of growth in the X_2–direction was balanced by subsequent growth in the X_3–direction. With reference to Fig. 5 of Part I the substituting semi-elliptic crack maintains the relation $a \approx b$ for its semi-axes. This is demonstrated in [2] and further confirmed by the calculated crack driving forces using the methodology described by Eq. (7) of Part I in the two directions, giving nearly identical development. In the absence of bridges, these crack driving forces coincide with the analytical predictions for stress intensity factors for semi-circular crack, given by Eq. (1) corrected for the finite geometry with Eq. (4) or Eq. (5) of Part I.

Fig. 2 shows an example of the development of the stress intensity factor (crack driving force) with crack area in a microstructure with f = 0.35. The stress intensity factor is determined via Eq. (7) of Part I in the X_3-direction and normalised as shown in the figure. In addition, the theoretical value for a semi-circular crack of the same semi-axes as the real crack is given, normalised accordingly. As the already the mentioned, the stress intensity in the X_2-direction follows closely the same curve as the one shown in the figure and the theoretical value is the latter in both directions.

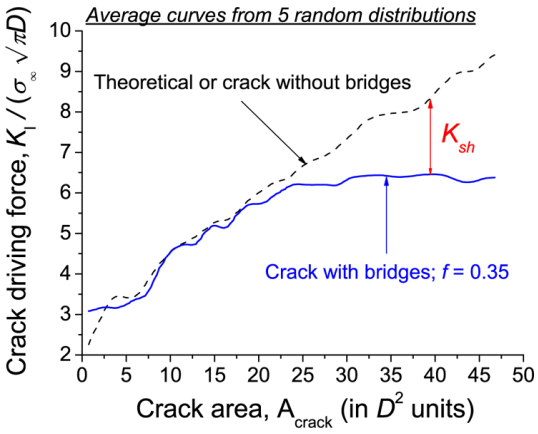

Figure 2. Crack driving force developments with crack advance in a microstructure with f = 0.35

Depicted with K_{sh} in the figure is the microstructure shielding effect, i.e. the difference between the crack driving force for an ideal plane semi-circular crack without bridges and the crack driving force determined in the real microstructure. For the crack extensions studied with the 3D model, the degree of crack branching out of the initial plane is minor, see Fig. 1(d), and correspondingly its contribution to the shielding effect is found to be insignificant. This is in some contrast to the results for 2D microstructures discussed later, where the shielding effect is shown to be a complex combination of the contributions from bridges and branches that depend on the fractions and failure properties of the susceptible and resistant boundaries. In the 3D case nearly the entire shielding effect of the microstructure is due to the bridges. Fig. 3 demonstrates this through the development of the stress intensity factor created by the bridges (crack bridging force) with respect to the crack front in the X_3-direction for three different microstructures, f = 0.25, 0.35, 0.45. The crack bridging forces are normalised similarly to the crack driving force in Fig. 2.

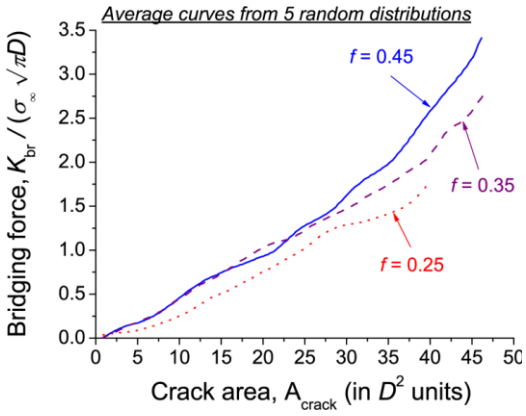

Figure 3. Crack bridging force developments with crack advance in selected microstructures

The effect of resistant boundaries fraction on the shielding effect is demonstrated in Fig. 4, where the results for K_{sh} for cracks of size $A_{crack} = 40D^2$ are plotted. It should be noted that this crack size developed close to termination points of the simulations corresponds to crack depths of 6-8 grains in different cases. These are short cracks compared to those studied with the 2D model, which did not allow for bridges to start yielding. There were very few exceptions to this, but in all cases the crack sizes were not sufficient to observe bridge failure. Hence, the shielding effect demonstrated in the figure is principally due to elastically strained bridges. The figure shows a nearly linear dependence of this shielding effect on the fractions of resistant boundaries. This is expected, because while the bridges are still in elastic regime and no failures occur, the shielding effect should be proportional to the total area of bridges (or their number in the present regular model), which is proportional to the fraction of resistant boundaries. The effect of yielding bridges and hence of resistant boundaries failure properties could be studied only with larger models and more extensive crack growth.

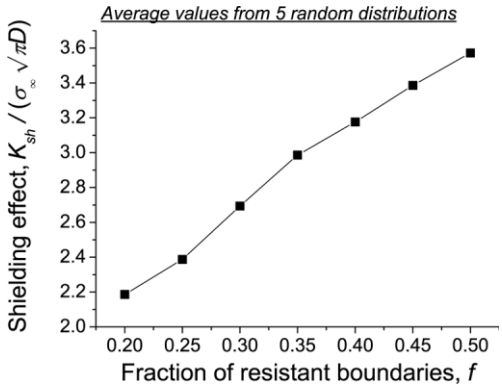

Figure 4. Dependence of shielding effect on resistant boundaries fraction

Although full parametric studies with 3D microstructures are not performed, the available results show that the model is capable of qualitatively reproducing crack advance and bridge formation. Simulations also show that in the region of interest for the resistant boundaries fraction, crack arrest is highly improbable. Due to the insufficient number of simulations with random distributions of boundaries for a given fraction, a deduction about the probability of arrest cannot be made. For the random distributions studied so far, crack arrest has not been achieved for any of the resistant boundaries fractions considered. Further, the effect of bridges is to decrease the crack driving force, with a consequent effect on crack growth rate, but their number is insufficient to lead to arrest. One may speculate at this stage that if crack arrest occurs in an assembly with the studied fractions of resistant boundaries it will be due to a rare distribution of resistant boundaries along the front of the propagating crack rather than due to the effect of bridges. The bridges, however, are expected to have impact via their shielding effect on the crack growth kinetics.

2.2. 2D Simulations

More extensive parametric studies have been performed with the 2D microstructure model. Fig. 5 gives an illustration for future reference of a crack grown in a microstructure with resistant boundaries fraction f = 0.3. Cracked boundaries are given with thick white lines and the red (thin) and blue (thick) lines show susceptible and resistant boundaries, respectively. The bridges formed by resistant boundaries and the crack branches are clearly identifiable.

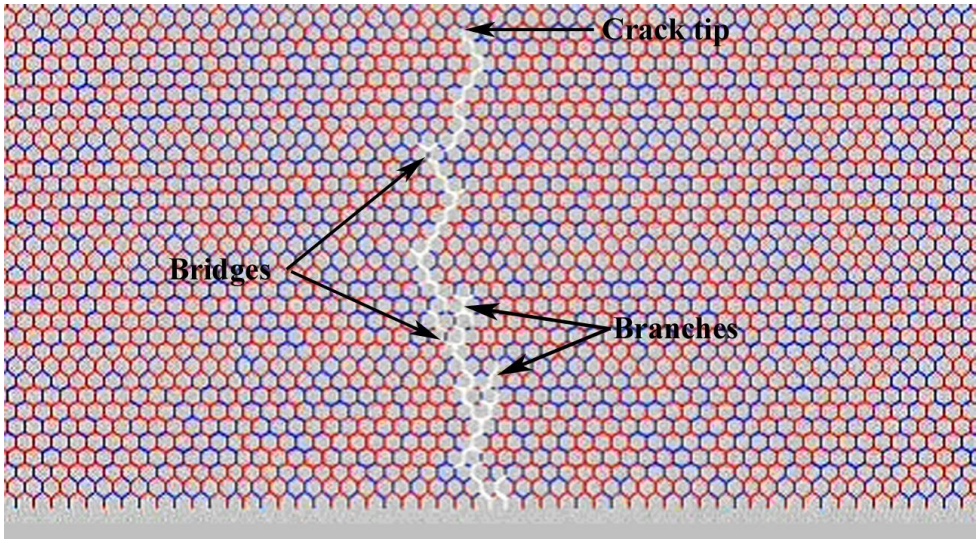

Figure 5. Crack propagated by "step" advance scheme in a hexagonal microstructure model

During simulations, the cracks have been allowed to propagate to a maximum extension a_{max} = 17D, which is a third of the assembly thickness in the crack propagation direction, W = 50D. Cracks reaching extension a_{max} are assumed to be percolating through the entire microstructure. This has been observed to be the case for all microstructures of interest, 0.25 < f < 0.40. Before focusing on this region of resistant boundaries fraction, it was advisable to check if the proposed mechanical model produces results that correlate sensibly with the existing results from percolation models. This has been reported in [3], where simulations with 2D geometry have been run for the full series of the resistant boundaries fraction, 0.1 ≤ f ≤ 0.9 and for a number of susceptible boundaries failure strains, ε_{sf} = 0, 0.1, 0.2 ε_0. The resistant boundaries failure strain has been fixed at ε_{rf} = 10ε_0. For each fraction f, 30 different random distributions of the boundaries have been considered and results have been averaged over these random distributions to give a single value for the given fraction. Fig. 6 presents the results for the achieved (at arrest) crack length a as a function of the resistant boundaries fraction, f. The crack length is normalised by the maximum allowed crack extension a_{max}. Note that unit normalised crack length should be interpreted as a crack percolated fully through the microstructure.

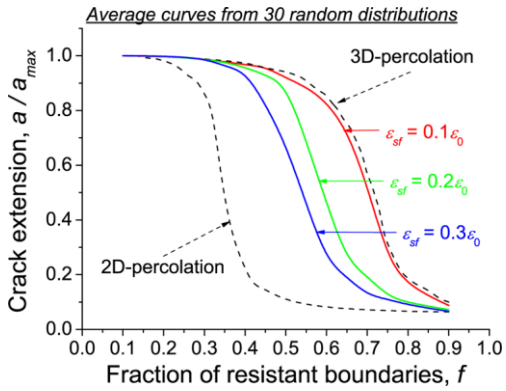

Figure 6. Crack extension as a function of resistant boundaries fraction.

Several observations have been made from these simulations. For a given fraction of susceptible boundaries, the crack arrest length determined by the 2D mechanical model is always smaller than the 3D percolation prediction and larger than the 2D percolation prediction. Decrease of the susceptible boundaries failure strain, ε_{sf}, leads to an increase of the arrest length, i.e. shift towards the 3D percolation prediction, as expected. Reversibly, increase of ε_{sf} shifts the arrest length towards the lower limit given by the 2D percolation prediction. This influence of ε_{sf}, however, is pronounced only for microstructures dominated by resistant boundaries, $f > 0.5$, and becomes insignificant for the microstructures of interest, $0.25 < f < 0.40$. In addition, ε_{sf} is a parameter that controls crack branching and this is again most pronounced for $f > 0.5$ [3]. For the series of fractions $0.2 \leq f \leq 0.5$ enclosing the region of interest as in the 3D case, in addition to the simulations with variable $\varepsilon_{sf} = 0.1, 0.2, 0.3, 0.4\ \varepsilon_0$ and fixed $\varepsilon_{rf} = 10\varepsilon_0$ described above, simulations for three values of resistant boundaries failure strain, $\varepsilon_{rf} = 5, 10, 50\ \varepsilon_0$, and fixed $\varepsilon_{sf} = 0.1\varepsilon_0$ have been performed. This has been done to assess the influence of ε_{rf}, since in the region of interest for f, the influence of ε_{sf} magnitude was estimated as small. The parameters that have been monitored are the projected crack length denoted by a, and the total crack surface, i.e. the main crack including branches and kinks, denoted by A.

For illustration, Fig. 7 gives the total number of bridges (a) and the number of yielding bridges (b) formed as the crack extends for the case with $\varepsilon_{sf} = 0.1\varepsilon_y$ and $\varepsilon_{rf} = 10$ and three selected fractions of resistant boundaries. The number of bridges is normalised with the projected crack length in terms of number of grains, $L = a / D$, while the crack extension, a, is normalised with the total assembly thickness, W. Values for the total number of bridges (N_{total}/L) in Fig. 7(a) that are larger than 1.0 indicate that there is a significant number of bridges formed not only along the main crack, but also along various crack branches. With the increasing of f, the number of branches decreases and N_{total}/L should become comparable to f. In theory, in the absence of branches, these two values must coincide, but this could be the case only if the crack has straight (zig-zag) geometry. In reality, with the increasing of f the crack has more opportunities to grow by kinking from the straight geometry and bridges form only when other possibilities are exhausted. This makes the value N_{total}/L smaller than expected on theoretical grounds, and this is visible in the curves for $f = 0.6$ and $f = 0.7$ in Fig. 7(a). Fig. 7(b) shows that the number of yielding bridges is much less dependent on the fraction of resistant boundaries in the region of interest and is more controlled by the current crack extension. It should be noted that decreases in the number of yielding bridges in Fig. 7(b), reflecting in decreases in the total number of bridges in Fig. 7(a), indicate failures of

yielding ligaments. These failures occur earlier, i.e. at shorter crack extensions, for smaller fractions of resistant boundaries, since the total number of bridges that are shielding the crack decreases.

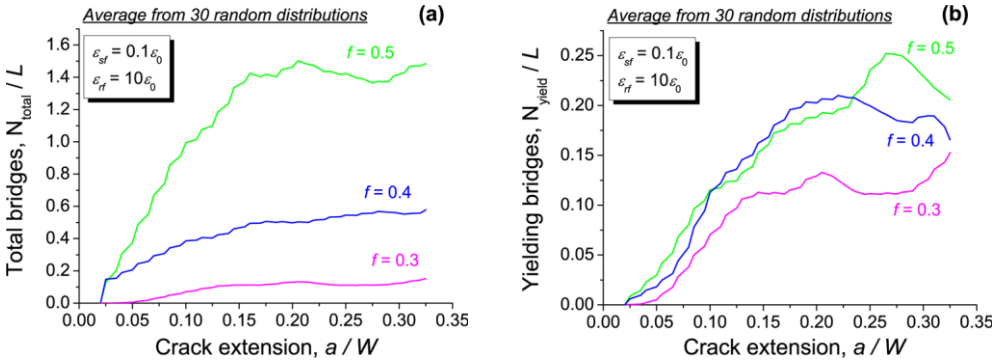

Figure 7. Average number of bridges (a) total and (b) yielding with crack extension

Fig. 8 gives the crack driving force (normalised stress intensity factor) evolution with crack extension for the case with $\varepsilon_{sf} = 0.1\varepsilon_y$ and $\varepsilon_{rf} = 10$ and four selected fractions of resistant boundaries. Crack extension, a, is again normalised with the total assembly thickness, W. Stress intensity factors are normalised as depicted in the figure, where σ_∞ stands for the actual remote stress in the structure. As the load is applied via prescribed displacements, the actual stress depends on the current stiffness of the cracked assembly and is found from the finite element solution. With crack advance, the remote stress decreases by 8% for the stiffest structure with $f = 0.5$ to 18% for the weakest structure with $f = 0.2$ in the interval of crack extensions shown in the figure. The stress intensity development is obtained through stress results from finite element solutions using Eq. (7), while the theoretical value is calculated using Eq. (9) of Part I. In the figure, K_{sh} denotes the shielding effect of the microstructure, which includes not only the effect of bridges but also the effect of branches on crack driving force reduction, as will become clear shortly.

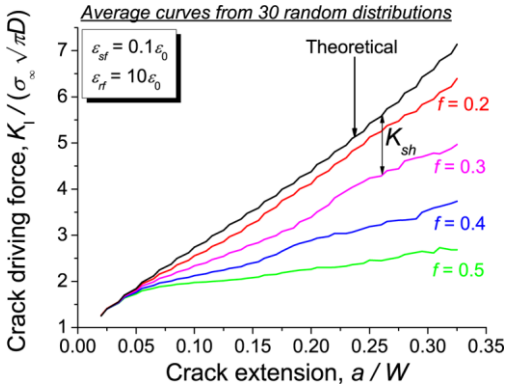

Figure 8. Stress intensity factors evolution with crack extension

The shielding effect is almost independent of the susceptible boundaries failure strain, ε_{sf}, but depends on the resistant boundaries failure strain, ε_{rf}, in the region of interest. This is demonstrated in Fig. 9, where the shielding stress intensity factor, K_{sh}, is plotted versus the

resistant boundaries fraction, f, for a selected crack extension, $a = 0.3W$, and for the series of failure strains of susceptible boundaries (a) and the series of failure strains of resistant boundaries (b). The stress intensity is normalised as in Fig. 8. The dependence on ε_{rf} comes from the larger contribution of bridges to the total shielding effect, which increases with the resistant boundaries failure strain.

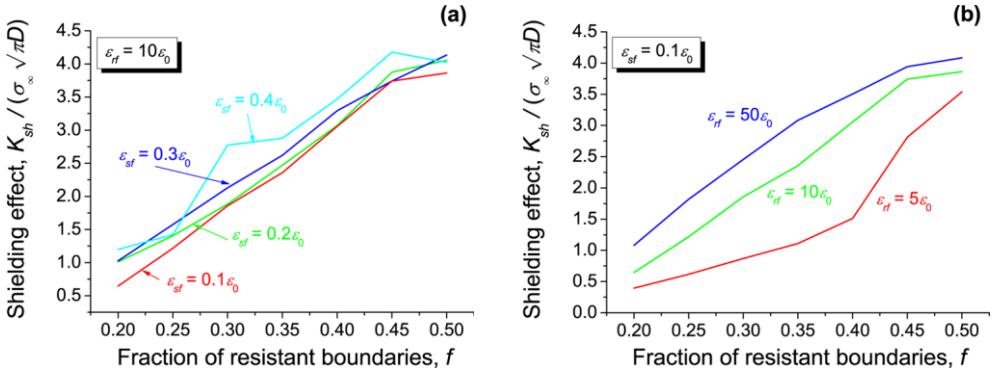

Figure 9. Shielding effect of microstructure with fraction *f*: (a) Susceptible boundaries failure strain effect; (b) Resistant boundaries failure strain effect

To quantify the relative effects of branching and bridging on the total shielding effect, the crack driving force reduction solely due to bridges has been estimated. This was done by calculating the stress intensity factors using Eq. (8) of Part I and the stress results from finite element solutions. As an illustration, Fig. 10 presents the stress intensity factors due to bridges alone for the same grain boundaries properties and fractions as in Fig. 8. The normalising factors for the two axes of the plot are also the same.

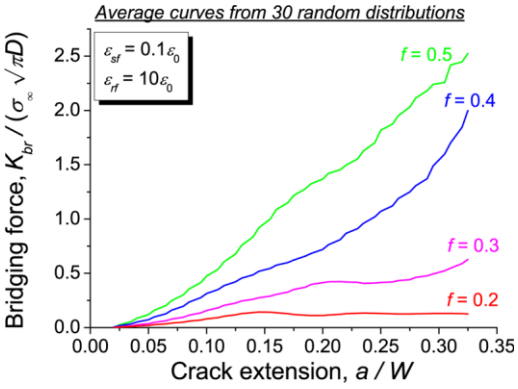

Figure 10. Bridging stress intensity factors evolution with crack extension

Fig. 11 demonstrates the effects of all bridges (a), only elastic bridges (b), and only yielding bridges (c) for the particular values of grain boundary properties depicted. Bridging effects are shown as fractions of the total shielding effect. The effect of elastic bridges is a non-linear increasing function of f, almost independent of ε_{rf}, while the effect of yielding bridges depends on ε_{rf}, and may turn into a decreasing function of f, for sufficiently large ε_{rf}. Thus, in the region of interest for f, yielding bridges provide the larger contribution to crack shielding and this relative contribution increases with increasing f.

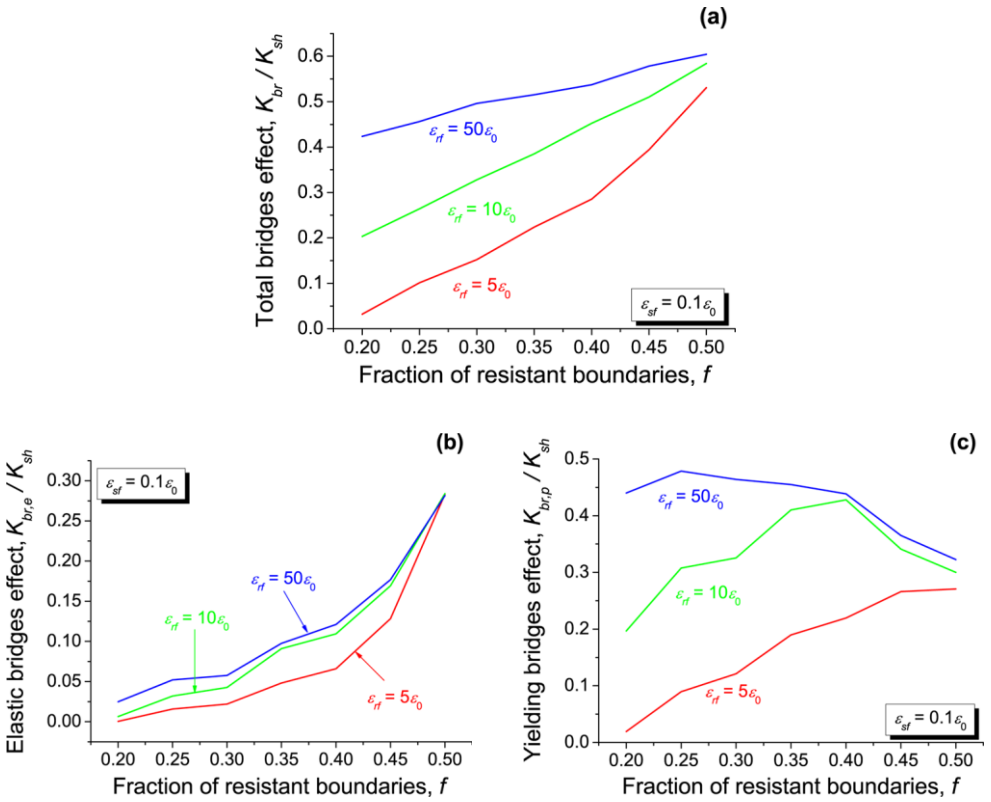

Figure 11. Contribution of all (a), elastic (b) and yielding (c) bridges to shielding effect

As a general observation from all the 2D simulations, the parameter controlling the effect of bridges is the resistant boundaries failure strain and the parameter controlling branching is the resistant boundaries fraction. The effect of the susceptible boundaries failure strain is negligible in the region of interest for fractions of resistant boundaries in the constraints of the model. The initial crack extension (pre-crack) and the applied load set a threshold for the susceptible boundaries failure strain above which the pre-crack cannot start propagating. For any value of the susceptible boundaries failure strain smaller than this threshold, cracks will propagate and will have the behaviour presented by the above results. Conversely, a fixed value of the susceptible boundaries failure strain will set a threshold on the applied load, below which cracks cannot start propagating. It may therefore be considered to be a material/environment parameter. According to the "jump" scheme for crack advance, a bridge can always form when a sub-exposed boundary is in a critical state, i.e. it is assumed that the real 3D microstructure will always allow for by-passing of a resistant boundary. Strictly this cannot be always the case, as it depends on the fraction and distribution of resistant boundaries in 3D. This means that a direct correspondence in the results from the 2D model and the 3D model at given f cannot be claimed. It is anticipated that results for given f obtained with the 2D model correspond to a 3D microstructure with smaller fraction of resistant boundaries. The precise correspondence between the 2D model and the 3D model remains to be determined, and would require more 3D simulations.

3. Conclusions

The proposed discrete structural model has the potential to simulate intergranular crack propagation in a realistic manner by including the phenomenon of crack bridging by ductile ligaments, formed by boundaries resistant to environmental attacks. It accounts for the effects of external load magnitude and the failure properties of the susceptible and the resistant boundaries. With the computational power available, the model is applicable to sufficiently large grain aggregates in two dimensions and to aggregates of limited size in three dimensions to represent an entire test specimen.

Development of bridges by resistant boundaries and their crack shielding effect has been demonstrated with the 3D microstructure model. In the region of practical interest for the fraction of resistant boundaries, the shielding effect was not sufficient to yield crack arrest, but increasing the fraction of resistant grain boundaries increased the degree of crack tip shielding developed. This would be expected to increase the resistance to stress corrosion crack propagation. Decreasing the grain size is also predicted to increase the resistance to intergranular stress corrosion cracking [2]. The 3D model has also been successfully used to study the coalescence of surface cracks [2]. It has been recently extended to account for kinetics of environment assisted failure of susceptible boundaries [4].

The parametric studies undertaken with the 2D model demonstrated the effects not only of the fraction of resistant boundaries, but also the effects of the failure properties of the susceptible and the resistant boundaries. Again, in the region of interest for resistant boundaries fraction, crack arrest was not observed, but a significant degree of crack tip shielding due to bridges and branches developed. The contributions of these two factors to the shielding effect were quantified. The failure properties of the susceptible boundaries were found to be unimportant for the development of the crack in the region of interest. They merely set a threshold for crack initiation given assembly geometry and loading. The fraction and failure properties of resistant boundaries were found to be the parameters that determine the shielding effects of branching and bridging. The 2D model has also been used to study the effects of grain size [5], and of residual stresses on crack propagation [6].

In summary, the overall resistance of a material to propagation of short intergranular cracks is predicted to be increased by grain boundary engineering that increases the fraction of resistant boundaries. Further refinement of the model requires that it be related to experimental observations of intergranular stress corrosion crack extensions and distributions to tune the model parameters. This is necessary in order to turn the model into a predictive tool. The results presented here will be useful as a guide for parameters identification.

ACKNOWLEDGEMENTS

The support of this research by Rolls-Royce Plc is highly appreciates. The opinions expressed in this paper are those of the author, and not necessarily those of the sponsor.

LITERATURE

1. *Marrow, T. J., L. Babout, A. P. Jivkov, P. Wood, D. Engelberg, N. Stevens, P. J. Withers, R. C. Newman*. Three dimensional observations and modelling of intergranular stress corrosion cracking in austenitic stainless steel. J. Nucl. Mater. 352: 62–74, 2006.
2. *Jivkov, A. P., N. P. C. Stevens, T. J. Marrow*. A three-dimensional computational model for intergranular cracking. Comput. Mater. Sci. 38: 442–453, 2006.
3. *Jivkov, A. P., N. P. C. Stevens, T. J. Marrow*. The roles of microstructure and mechanics in intergranular stress corrosion cracking. In: Simulation of electrochemical processes, 217–226. Brebbia, C. A., V. G. DeGiorgi, R. A. Adey (Eds.). Proc. 1st Int. Conf. Simulation of Electrochemical processes, May 2–4, 2005, Cadiz, Spain.
4. *Jivkov, A. P., N. P. C. Stevens, T. J. Marrow*. Modelling intergranular stress corrosion cracking in simulated three-dimensional microstructures. Submitted to Key Eng. Mater.
5. *Jivkov, A. P., N. P. C. Stevens, T. J. Marrow*. Meso-mechanical model for intergranular stress corrosion cracking and implications for microstructure engineering. J. Pres. Vess. Tech.-Trans. ASME, in press, 2007.
6. *Marrow, T. J., D. Engelberg, A. P. Jivkov, P. Wood, L. Babout, N. P. C. Stevens*. Grain boundary control for improved intergranular stress corrosion cracking resistance in austenitic stainless steels. Energy Materials: Mater. Sci. Eng. Energy Systems 1: 98–102, 2006.

Submitted: March 2007

МОДЕЛИРАНЕ НА МЕЖДУЗЪРНЕСТ РАСТЕЖ НА ПУКНАТИНИ В ПОМОЩ НА МИКРОСТРУКТУРНОТО ИНЖЕНЕРСТВО. ЧАСТ II: РЕЗУЛТАТИ

А. Живков[1]

Ключови думи: *корозионно напукване, геометрия на пукнатината, зараждане на пукнатина, еволюция на пукнатина, задачи с подвижни граници, крайни елементи*

MSC 2000: *74R10*

РЕЗЮМЕ

Представени са резултати за растежа на пукнатина в пространствения модел за серия от експериментално измерени дялове на устойчивите междузърнести граници. Резултатите демонстрират образуването на мостове от устойчивите граници и тяхното влияние върху движещата сила за растеж на пукнатината. Показано е, че увеличаването на дела на устойчивите граници води до увеличаване на степента на защита на пукнатината. Развитата защита се очаква да понижи скоростта на растеж на пукнатината и оттам да повиши устойчивостта на материала на междузърнестото напукване. С равнинния модел са направени симулации със случайни разпределения на междузърнестите граници в микроструктурата за серия от якости на разрушаване на устойчивите и на податливите граници. Демонстрирани са влиянието на напраженията върху морфологията на пукнатината и влиянието на якостите на разрушение на устойчивите и податливите граници върху поведението на пукнатината. Ефектите на премостването и на разклоненията на пукнатината са изразени количествено. Заключено е, че защитният ефект на мостовете се определя от дела и от характеристиката на разрушаване на устойчивите граници.

Постъпила: март 2007

[1] Андрей Живков, The University of Manchester, School of Materials, Grosvenor Street, Manchester M1 7HS, UK; Tel: +44 (0)161 3063556; Fax: +44 (0)161 3063586; E-mail: andrey.jivkov@manchester.ac.uk